



Effect of the synthesis temperature on the dimensionality of hybrid fluorozincates



Vanessa Pimenta, Quang Hoang Hanh Le, Annie Hemon-Ribaud, Marc Leblanc, Vincent Maisonneuve, Jérôme Lhoste*

LUNAM Université, Université du Maine, CNRS UMR 6283, Institut des Molécules et Matériaux du Mans (IMMM), Avenue Olivier Messiaen, 72085 Le Mans Cedex 9, France

ARTICLE INFO

Article history:

Received 26 May 2016
Received in revised form 4 July 2016
Accepted 7 July 2016
Available online 11 July 2016

Keywords:

Hybrid fluoride
Tetrazole
MOF
Solvothermal synthesis
Microwave heating

ABSTRACT

A series of new hybrid fluorozincates incorporating 5-aminotetrazole (*Hamtetraz*) is obtained from a same starting mixture of ZnF_2 , HF solution and *Hamtetraz* in acetonitrile at different synthesis temperatures. The structures, determined by single crystal X-ray diffraction, exhibit various networks with dimensionalities that increase as a function of the synthesis temperature. At 120 °C, two phases, $ZnF_2(H_2O)(Hamtetraz)$ (**1**) and $ZnF_2(Hamtetraz)_2$ (**2**), coexist and display 1D infinite chains. $\infty [ZnN_2F_2O]$ chains are built up from $ZnN_2F_3(H_2O)$ octahedra linked by opposite fluorine corners in **1**, while $\infty [ZnN_2F_2]$ chains of edge sharing ZnN_2F_4 octahedra are found in **2**. At 130 °C, dense layers appear in $Zn_3F_5(H_2O)_2(amtetraz)$ (**3**); they result from the condensation of $\infty [ZnF_3N_2]$ and $\infty [ZnF_2NO]$ chains by fluorine corners to form a neutral 2D network. At 140 °C, $[NH_4] \cdot (Zn_4F_5(amtetraz)_4) \cdot 3H_2O$ (**4**) presents an anionic 3D network containing small cavities in which water molecules and ammonium cations are inserted. The thermal behavior of the coordination polymers **3** and **4** is studied by TGA analysis and X-ray thermodiffraction; an intermediate phase is observed during the decomposition of **4**.

© 2016 Elsevier B.V. All rights reserved.

1. Introduction

Hybrid inorganic–organic porous materials, also called porous coordination polymers (PCPs) or metal–organic frameworks (MOFs), represent a new generation of crystalline multifunctional porous materials with potential applications in numerous fields, such as energy or health [1,2]. The PCPs, considered as supramolecular compounds with zeolite-like architectures, are built up from inorganic units and organic linkers that lead eventually to 3D frameworks with large cavities giving high surface area. Consequently, these porous materials can show exceptional catalytic and gas storage properties [3,4]. The first explored properties of MOFs were focused on adsorption of H_2 or CH_4 which could be used as future energy sources [5,6]. Nonetheless, CO_2 capture [7] and gas separation [8] are also seen as promising applications. The adsorption properties of these architectures are strongly influenced by numerous parameters such as the size and the topology of the organic linkers [9] or the presence of unsaturated metal sites known to be a key factor in gas adsorption [10]. To tune the network's topology, the most common approach consists to modify the

chemical nature of the precursors: organic linkers, metal cations or counterions [11]. Depending on the transition metal ions and its oxidation states, numerous coordination numbers from 2 to 7 give multiple geometries leading to original network topologies. The coordination numbers and the orientation of linker binding sites can also modify the network topologies and influence the size and shape of pores. The influence of metal cations and linkers has been largely demonstrated for MOFs containing carboxylate ligands [12]. As examples, MIL-53 [13] and MOF-5 [14] are prepared with benzenedicarboxylate ligands and Cr^{3+} and Zn^{2+} cations respectively. Ouellette et al. reported six new structures in the Cd(II)-1,2,4-triazolate system by changing the counterion nature only (F^- , Cl^- , Br^- , I^- , SO_4^{2-} and NO_3^-) [15]. It must be noted that the metal complexes with azoles as organic ligands are called Metal Azolate Frameworks (MAFs).

In the present work, we focus on the synthesis of hybrid fluorides with Zn^{2+} cation and aminotetrazole (*Hamtetraz*) as linker. The deprotonated form of aminotetrazole (*amtetraz*)⁻, that presents an aromatic cycle with four nitrogen donor atoms to form N–M bonds, is preferred in order to promote high network dimensionality. The values of deprotonation acidic constants of *Hamtetraz/amtetraz*⁻ couple ($pK_A = 4.6$) and the HF/F^- couple ($pK_A = 3.2$) are very close; this feature favours the crystallization of fluorinated MAFs. Zn^{2+} cation is selected for its aptitude to accept

* Corresponding author.

E-mail address: jerome.lhoste@univ-lemans.fr (J. Lhoste).

different coordination geometries, from a tetrahedral environment to an octahedral geometry. Suh et al. have reported the synthesis of Zn-based networks in which the Zn²⁺ coordination reversibly changes from trigonal bipyramidal to tetrahedral geometry by a desolvation/solvation mechanism [16]. Therefore, it is expected that the association of tetrazole cycles, fluoride ions and unsaturated metal sites in porous materials will be propitious to the gas uptake. While the literature is rich in terms of azole compounds, the presence of fluoride counterions is sparse. Thirteen metalate hybrids with fluorinated 2D or 3D networks are reported to date; six phases integrate only Zn²⁺ cations [17–21] and seven others combine divalent cations (Fe²⁺, Zn²⁺, Ni²⁺) associated to trivalent cations (A = Al³⁺, Fe³⁺) [17,22,23–25]. Most of the reported compounds are elaborated from 1,2,4-triazole or derivatives and they are generally obtained by solvothermal synthesis. While it is well known that the choice of the solvent or the reaction temperature allows the control of the network dimensionalities and topologies of metal carboxylates [26,27], the effects of the synthesis parameters are rarely described for fluorinated hybrids with nitrogen ligands. We have recently evidenced 3D networks that are obtained in acidic conditions and low azole concentrations [17,22,23]. Following an equivalent synthesis strategy, this paper reports on four new compounds with *Hamtetraz* and Zn²⁺ cations obtained by changing the synthesis temperature only: ZnF₂(H₂O)(*Hamtetraz*) (1) and ZnF₂(*Hamtetraz*)₂ (2) at 120 °C, Zn₃F₅(H₂O)₂(*amtetraz*) (3) at 130 °C and [NH₄](Zn₄F₅(*amtetraz*)₄)·3H₂O (4) at 140 °C. It is demonstrated that the increase of the synthesis temperature results in increased network dimensionality. We first describe the structures and the entities condensation. Then, the thermal behavior of 3 and 4 is studied and it is evidenced that 4 presents a crystalline intermediate with possible unsaturated metal sites.

2. Results and discussion

2.1. Crystal structure description

Four new hybrid fluorozincates are obtained by solvothermal synthesis at different temperature: ZnF₂(H₂O)(*Hamtetraz*) (1) and ZnF₂(*Hamtetraz*)₂ (2) at 120 °C, Zn₃F₅(H₂O)₂(*amtetraz*) (3) at 130 °C and [NH₄](Zn₄F₅(*amtetraz*)₄)·3H₂O (4) at 140 °C. The structures are determined from single crystal X-ray diffraction data. Details of the structure determinations are given in Table 1. Selected interatomic distances of zincate and organic groups are gathered in Table 2.

The structure of 1 is built up from neutral *trans*-chains ∞[ZnF₂N₂O] oriented along the *b* axis (Fig. 1 left). These chains contain ZnF₃N₂O octahedra connected by fluorine atoms F(2) and by *Hamtetraz* in the N1,N2-bridging mode [17] (Scheme S1). The presence of water molecule is confirmed by a long distance to Zn²⁺ (2.16 Å) compared to Zn–F(1) (2.10 Å). Fluoride ions, hydrogen atoms of –NH₂ of *Hamtetraz* and coordinated water molecules ensure the stability of the structure (Fig. 1 right) via hydrogen bonds (2.61–2.98 Å).

In 2, the condensation of (ZnF₄N₂) units by the connection of F–F edges gives infinite ∞[ZnF₂(*Hamtetraz*)₂] chains oriented along *a* axis (Fig. 2 left). Nitrogen atoms of neutral tetrazole cycles, in N1-bridging mode, occupy the axial positions of the octahedra. Hydrogen bonds contribute to the stability of the structure with N–H···F(1) (2.58 and 2.89 Å) and N–H···N (3.16 Å) intra- and inter-chain interactions (Fig. 2 right).

The crystal system of 3 is orthorhombic with *Fmmm* space group. The architecture results from the stacking of (001) sheets linked by interlayer bonds Ow–H···Ow (2.58 Å) along the *c* axis (Fig. 3 left). The sheet can be described from inorganic 1D [100] columns (Fig. 3 right) connected by deprotonated aminotetrazole

Table 1

Crystallographic data of ZnF₂(H₂O)(*Hamtetraz*) (1), ZnF₂(*Hamtetraz*)₂ (2), Zn₃F₅(H₂O)₂(*amtetraz*) (3) and [NH₄](Zn₄F₅(*amtetraz*)₄)·3H₂O (4) at room temperature.

Formula	1	2	3	4
	ZnF ₂ ON ₅ CH ₅	ZnF ₂ N ₁₀ C ₂ H ₆	Zn ₃ F ₅ O ₂ N ₅ CH ₆	Zn ₄ F ₅ O ₃ N ₂₁ C ₄ H ₁₂
<i>M</i>	206.47	273.52	411.25	758.83
Crystal system	orthorhombic	monoclinic	orthorhombic	monoclinic
ρ _{calc} (g cm ^{−3})	2.331	2.222	3.098	2.260
Space group	<i>P2₁2₁2₁</i>	<i>P2₁/n</i>	<i>Fmmm</i>	<i>P2₁/c</i>
<i>a</i> (Å)	6.2611(6)	3.2988(1)	3.9732(18)	6.5873(1)
<i>b</i> (Å)	6.9066(5)	12.2103(4)	17.551(7)	12.9396(3)
<i>c</i> (Å)	13.6068(13)	10.2295(3)	25.28(2)	13.0141(3)
β (°)	–	97.205(2)	–	90.023(1)
<i>V</i> (Å ³)	588.4(1)	408.8(1)	1762.8(13)	1109.3(1)
<i>Z</i>	4	2	8	2
μ(Mo, Kα) (mm ^{−1})	4.152	3.026	8.175	4.374
<i>F</i> (000)	408	272	1552	730
No. of unique reflns	1712	2476	1171	2542
No. of obsd reflns [<i>I</i> > 2σ(<i>I</i>)]	1130	2157	956	2469
Refined parameters	98	70	53	162
GOF	0.999	1.266	1.257	1.250
Final R indices [<i>I</i> > 2σ(<i>I</i>)]	R ₁ = 0.0428 wR ₂ = 0.0771	R ₁ = 0.0632 wR ₂ = 0.1737	R ₁ = 0.0486 wR ₂ = 0.1431	R ₁ = 0.0513 wR ₂ = 0.1428
R indices (all data)	R ₁ = 0.0738 wR ₂ = 0.0881	R ₁ = 0.0685 wR ₂ = 0.1767	R ₁ = 0.0660 wR ₂ = 0.1675	R ₁ = 0.0523 wR ₂ = 0.1441
Largest diff. peak and hole (e [−] /Å ³)	−0.496, 0.510	−1.025, 4.708	−1.614, 1.559	−0.863, 4.026

Crystallographic data (excluding structure factors) for all structures have been deposited at the Cambridge Crystallographic Data Centre, CCDC 1446241 (ZnF₂(H₂O)(*Hamtetraz*) (1)), 1044011 (ZnF₂(*Hamtetraz*)₂ (2)), 1044009 (Zn₃F₅(H₂O)₂(*amtetraz*) (3)) and 1044010 ([NH₄](Zn₄F₅(*amtetraz*)₄)·3H₂O (4)). Copies of the data can be obtained, free of charge, on application to CCDC, 12 Union Road, Cambridge CB2 1EZ, UK, (fax: +44 1223 336033 or e-mail: deposit@ccdc.cam.ac.uk).

Table 2

Selected inter-atomic distances of zincate and organic groups in $\text{ZnF}_2(\text{H}_2\text{O})$ (*Hamtetraz*) (1), $\text{ZnF}_2(\text{Hamtetraz})_2$ (2), $\text{Zn}_3\text{F}_5(\text{H}_2\text{O})_2(\text{amtetraz})$ (3) and $[\text{NH}_4]\cdot(\text{Zn}_4\text{F}_5(\text{amtetraz}))\cdot 3\text{H}_2\text{O}$ (4).

	Zincate groups		Organic groups	
1	Zn(1)-F(2)	2.004(2)	N(1)-C(1)	1.329(6)
	Zn(1)-F(2)	2.005(2)	N(1)-N(2)	1.362(5)
	Zn(1)-F(1)	2.099(3)	N(2)-N(3)	1.285(5)
	Zn(1)-N(1)	2.113(4)	N(3)-N(4)	1.345(6)
	Zn(1)-OW(1)	2.157(4)	N(4)-C(1)	1.330(6)
2	Zn(1)-N(2)	2.160(4)	N(5)-C(1)	1.346(7)
	Zn(1)-N(4) x2	2.052(2)	N(4)-C(1)	1.336(3)
	Zn(1)-F(1) x2	2.099(2)	N(4)-N(3)	1.360(3)
	Zn(1)-F(1) x2	2.161(2)	N(3)-N(2)	1.280(4)
3			N(1)-C(1)	1.338(4)
	Zn(1)-F(3) x2	1.990(1)	N(1)-N(2)	1.354(4)
	Zn(1)-F(1) x2	2.103(5)	C(1)-N(5)	1.338(4)
	Zn(1)-N(1) x2	2.149(5)	N(1)-N(1)	1.30(1)
	Zn(2)-OW(1)	2.000(5)	N(1)-N(2)	1.377(8)
	Zn(2)-F(2) x2	2.029(1)	N(2)-C(1)	1.348(8)
	Zn(2)-N(2)	2.060(6)	C(1)-N(3)	1.34(2)
	Zn(2)-F(1)	2.120(5)	C(1)-N(2)	1.348(8)
	Zn(2)-F(2)	2.162(5)		
	4	Zn(1)-F(3) x2	2.015(4)	N(1)-C(1)
Zn(1)-N(8) x2		2.163(7)	N(1)-N(2)	1.354(8)
Zn(1)-N(3) x2		2.158(6)	N(2)-N(3)	1.298(9)
Zn(2)-F(2)		1.957(4)	N(3)-N(4)	1.335(9)
Zn(2)-N(6)		2.008(6)	N(4)-C(1)	1.310(9)
Zn(2)-N(1)		2.021(5)	C(1)-N(5)	1.37(1)
Zn(2)-F(2)		2.081(4)	N(6)-C(2)	1.35(1)
Zn(2)-F(1)		2.127(1)	N(6)-N(7)	1.36(1)
Zn(3)-F(3) x2		2.047(4)	N(7)-N(8)	1.31(1)
Zn(3)-N(4) x2		2.132(6)	N(8)-N(9)	1.33(1)
Zn(3)-N(9) x2		2.169(7)	N(9)-C(2)	1.30(1)
			C(2)-N(10)	1.36(1)

(*amtetraz*)⁻ along *b* (Fig. 3 left and right). Two types of chains, corresponding to two crystallographic independent Zn^{2+} sites, 8 h (Zn(1)) and 16 m (Zn(2)), built up the inorganic columns (Fig. 4 right). Corner sharing $\text{Zn}(1)\text{F}_4\text{N}_2$ octahedra linked by opposite

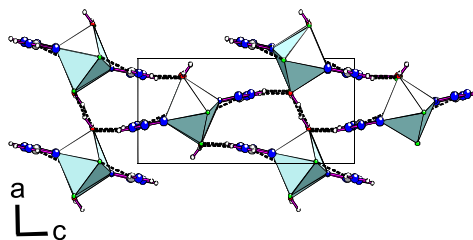
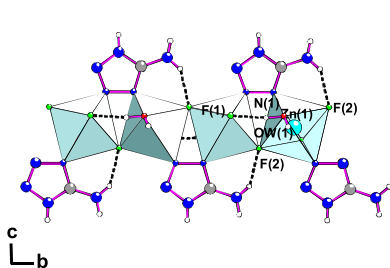


Fig. 1. $\infty[\text{ZnF}_2\text{N}_2\text{O}]$ chain (left) and [010] projection (right) of $\text{ZnF}_2(\text{H}_2\text{O})(\text{Hamtetraz})$ (1). Dashed lines represent the hydrogen bonds.

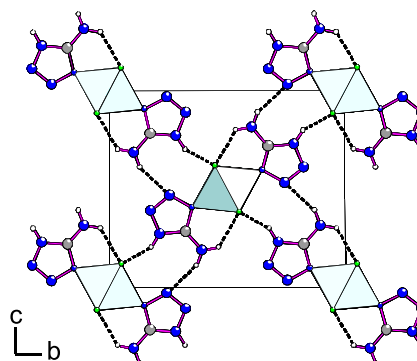
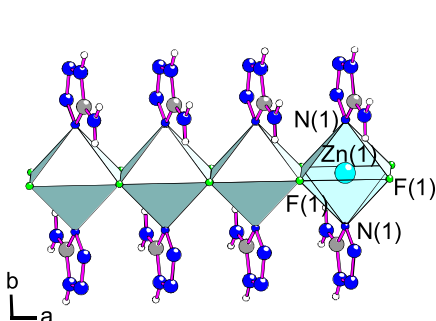


Fig. 2. $\infty[\text{ZnF}_2\text{N}_2]$ chain (left) and [100] projection (right) of $\text{ZnF}_2(\text{Hamtetraz})_2$ (2). Dashed lines represent the hydrogen bonds.

fluorine atoms (F(3)) result in an infinite *trans*-chain $\infty[\text{ZnF}_3\text{N}_2]$ (Fig. 4 left). In the second chain, $\text{Zn}(2)\text{F}_4\text{NO}$ octahedra are linked to two neighboring octahedra by two adjacent F–F edges and form a zigzag chain $\infty[\text{ZnF}_2\text{NO}]$ (Fig. 4 middle). The connection of these chains by fluorine atoms F(1) and tetrazolate in N1,N2,N3,N4-bridging mode leads to a very compact network ($\rho = 3.098 \text{ g cm}^{-3}$). Consequently, the bidimensional compound **3** does not contain any accessible porosity.

The structure of **4**, obtained at the highest synthesis temperature, exhibits an anionic 3D framework with square tunnels along [100] in which water molecules and ammonium cations are inserted (Fig. 5 left). The oxygen or nitrogen atoms of isolated species are statically disordered and are located on Ow(1)/N(11) and Ow(2)/N(12) sites with O/N ratio equal to 0.75/0.25. The structure results from two types of [100] chains, connected by (*amtetraz*)⁻ anions in the N1,N2,N4-bridging modes (Fig. 5 right). These chains contain alternating ZnF_2N_4 monomers or $\text{Zn}_2\text{F}_4\text{N}_4$ dimers linked by opposite fluorine corners to form infinite $\infty[\text{ZnFN}_4]$ and $\infty[\text{Zn}_2\text{F}_3\text{N}_4]$ chains, respectively. The metal cations adopt an octahedral geometry in ZnF_2N_4 and a trigonal bipyramidal geometry in $\text{Zn}_2\text{F}_4\text{N}_4$. These chains were recently mentioned in [Hdma]·($\text{Zn}_4\text{F}_5(\text{amtetraz})_4$) [17].

2.2. Influence of the synthesis temperature on the network dimensionality

Four new fluorozincates have been prepared from the same starting mixture at different temperatures. At 120 °C, $\text{ZnF}_2(\text{H}_2\text{O})$ (*Hamtetraz*) (1) and $\text{ZnF}_2(\text{Hamtetraz})_2$ (2) develop 1D networks in which the aminotetrazole linker is neutral. In **1**, the N1,N2-bridging mode is observed; the linker acts as a bridging ligand between two metallic centres with a ratio $\text{Zn}/\text{Hamtetraz}$ equal to 1. In **2**, *Hamtetraz* establishes only one N–M bond in N1-bridging mode, and the $\text{Zn}/\text{Hamtetraz}$ ratio is 1/2. At 130 °C, the tetrazole ligand is deprotonated and displays a N1,N2,N3,N4-bridging mode in the 2D network of $\text{Zn}_3\text{F}_5(\text{H}_2\text{O})_2(\text{amtetraz})$ (3); the $\text{Zn}/\text{amtetraz}$ ratio is 3. This (*amtetraz*)⁻ deprotonated form is also observed in the 3D

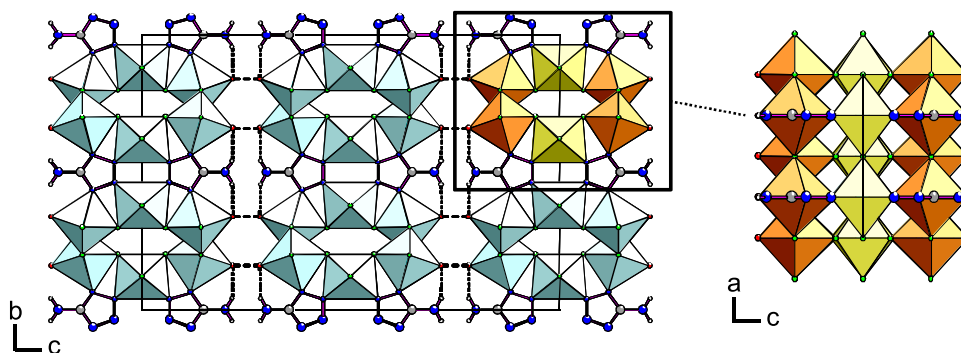


Fig. 3. [100] projection of $\text{Zn}_3\text{F}_5(\text{H}_2\text{O})_2(\text{amtetraz})$ (**3**) (left) and [010] projection of inorganic column in **3** (right). Dashed lines represent the hydrogen bonds.

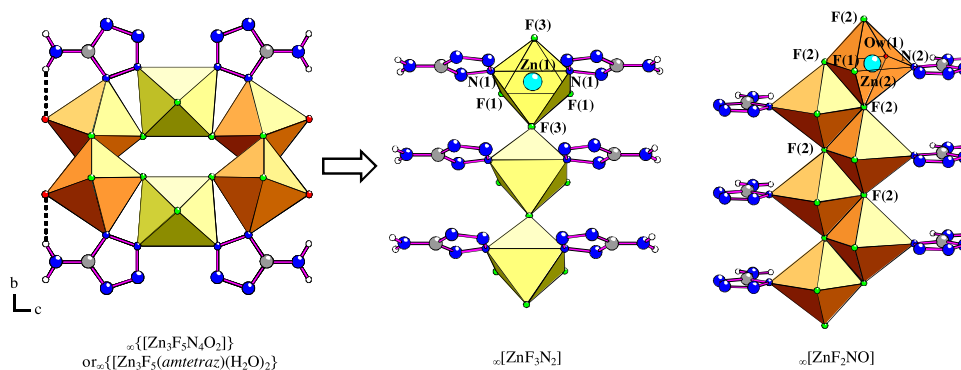


Fig. 4. View of $\infty[\text{ZnF}_3\text{N}_2]$ (left) and $\infty[\text{ZnF}_2\text{NO}]$ chains (middle) observed in inorganic 1D [100] columns (right) of **3**.

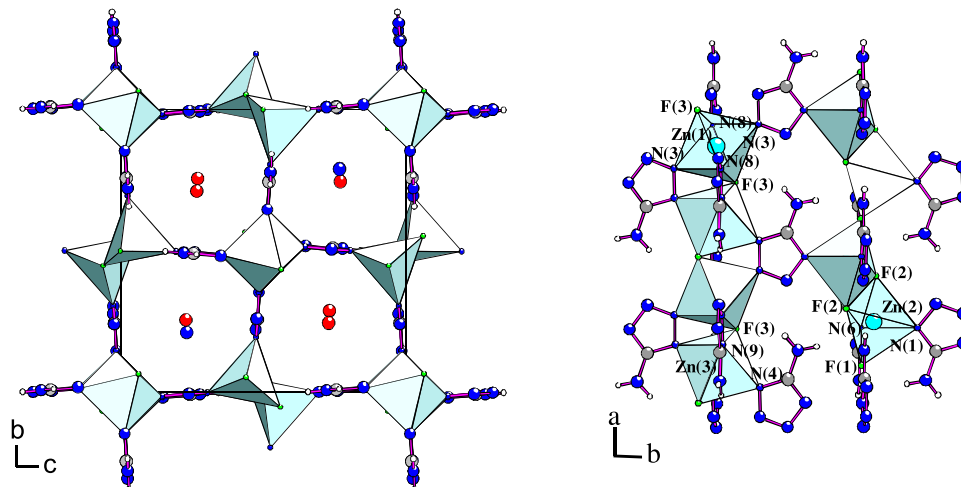


Fig. 5. [100] projection of $[\text{NH}_4] \cdot (\text{Zn}_4\text{F}_5(\text{amtetraz})_4) \cdot 3\text{H}_2\text{O}$ (**4**) (left) and connection of the [100] chains (right).

network of $[\text{NH}_4] \cdot (\text{Zn}_4\text{F}_5(\text{amtetraz})_4) \cdot 3\text{H}_2\text{O}$ (**4**), prepared at 140°C . In this case, the linker, in N1,N2,N4-bridging mode, ensures the connectivity between three Zn^{2+} cations; the Zn/amtetraz ratio is equal to 1. It clearly appears that the increase of the synthesis temperature leads to the condensation of metal entities and the increase of the dimensionality. Two effects influence the formation of the solids: the partial decomposition of tetrazole and the competition for the metal complexation. At highest temperature, a part of *Hamtetraz* decomposes into ammonia which increases the pH of the reaction media [28,29]. Consequently, the aminotetrazole is deprotonated, with four available electron-donor N atoms, promoting the establishment of N–M bonds and a high

dimensionality. The second effect concerns the metal complexation; the aminotetrazolate anions are in competition with aqua ligands. At 130°C , **3** contains two coordinated water molecules and one azolate per three zinc atoms. At 140°C , water molecules are replaced by nitrogen atoms giving **4** with one organic molecule per one zinc atom.

2.3. Thermal behaviour of **3** and **4** and infrared spectra analysis for **4**

The TG curve of $\text{Zn}_3\text{F}_5(\text{H}_2\text{O})_2(\text{amtetraz})$ shows three successive weight losses (Fig. 6). The first step between 180°C and 260°C is attributed to the dehydration of **3** (exp.: 8.9%, calc. 8.8%). Then, the

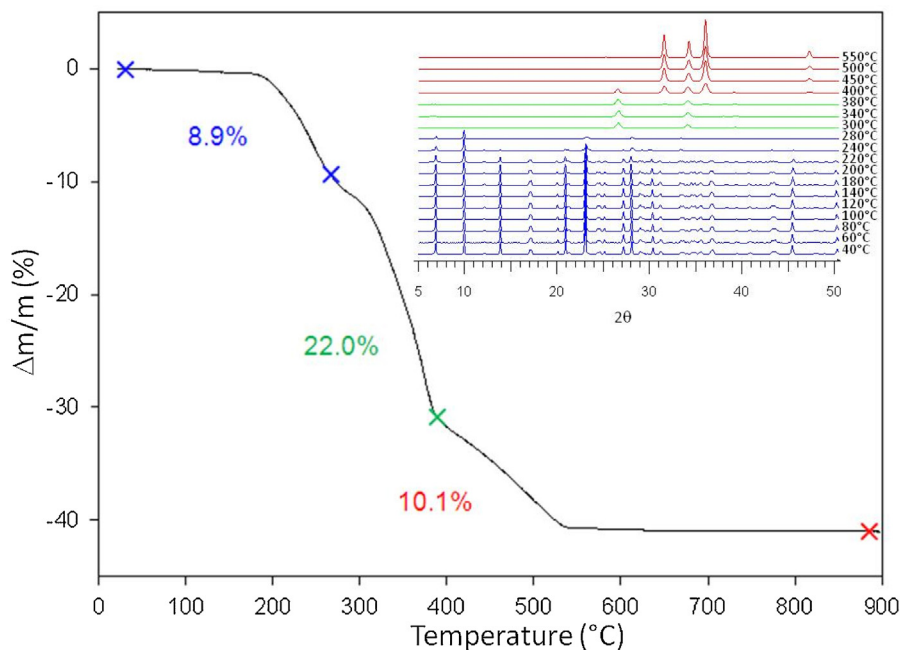


Fig. 6. Thermogravimetric analysis and thermal evolution of the X-ray diffractograms of $\text{Zn}_3\text{F}_5(\text{H}_2\text{O})_2(\text{amtetraz})$ (**3**) under air at 2°C min^{-1} .

second weight loss, up to 380°C , corresponds to the loss of tetrazole linkers and HF gas, leading to the formation of ZnO and ZnF_2 (exp.: 22.0%, calc. 21.2%). At 900°C , ZnF_2 is totally hydrolysed in zinc oxide (exp.: 10.1%, calc. 10.7%). X-ray thermodiffraction shows three domains (Fig. 6). **3** is stable up to 180°C ; the loss of two water molecules between 180°C and 280°C results in the formation of a quasi-amorphous phase. Above 280°C , ZnF_2 appears and is gradually transformed to ZnO above 380°C .

Three successive weight losses are also observed on the TG curve of **4**. The first event, between 130°C and 220°C , corresponds to the loss of three water molecules and one ammonium fluoride

(exp.: 12.7%, calc. 12.0%). A plateau is observed up to 340°C and is compatible with the existence of an intermediate phase. Then, a second weight loss, in which the fluoride entities and a part of the organic ligands are eliminated, leads to the formation of $\text{Zn}(\text{CN})_2$ at 360°C (exp.: 31.8%, calc. 32.9%). The last weight loss is assigned to the hydrolysis of zinc cyanide to zinc oxide (exp.: 12.4%, calc. 12.5%). X-ray thermodiffraction is in good agreement with TG analyses and confirms the existence of an intermediate compound (Fig. 7). The initial phase is stable up to 140°C ; above this temperature, a shift of the peaks positions toward larger angles occurs together with a variation of the intensities. These features

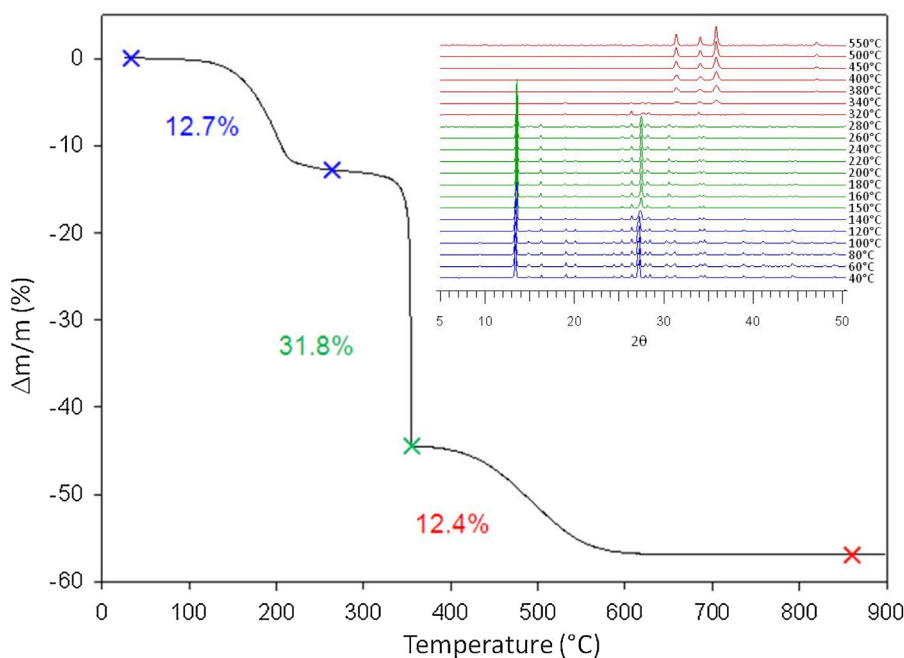


Fig. 7. Thermogravimetric analysis and thermal evolution of the X-ray diffractograms of $[\text{NH}_4] \cdot (\text{Zn}_4\text{F}_5(\text{amtetraz})_4) \cdot 3\text{H}_2\text{O}$ (**4**) under air at 2°C min^{-1} .

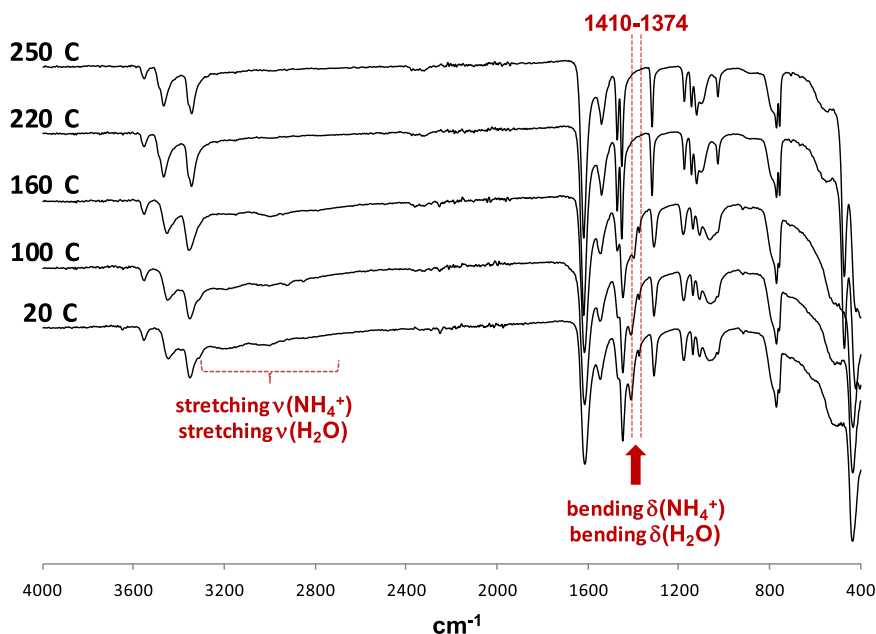


Fig. 8. Evolution of the infrared spectra of $[\text{NH}_4]\cdot(\text{Zn}_4\text{F}_5(\text{amtetraz})_4)\cdot 3\text{H}_2\text{O}$ (**4**) after treatment at increasing temperatures under air atmosphere.

are consistent with the appearance of a crystalline intermediate between 140 °C and 280 °C after the loss of NH_4F and H_2O . At high temperature, ZnO is formed.

To evidence the presence and the elimination of ammonium cations and water molecules in **4** on heating, IR spectra were collected after heating at increasing temperatures under air and cooling to room temperature. The spectra show two domains of vibrational N–H and O–H energy [30]. The first domain between 3200 and 2810 cm^{-1} and the second domain around 1400 cm^{-1} are respectively assigned to stretching vibrations and bending vibrations (Fig. 8). When the heating temperature increases several bands progressively disappear, which is in agreement with the elimination of the NH_4^+ and H_2O species. At 220 °C, the ammonium cations and water molecules are totally removed.

The results obtained for **4** by thermal analyses and IR spectroscopy confirm the existence of a crystalline intermediate that is strongly structurally related to **4** after elimination of H_2O and NH_4F . X-ray thermogravimetry shows that the structure is globally maintained and a possible chemical formula for the intermediate compound is $\text{ZnF}(\text{amtetraz})$. It can be assumed that this phase contains unsaturated zinc coordination sites, known to exacerbate gas adsorption; the theoretical porosity is estimated to 24%. In order to confirm this hypothetical formulation, the structure is under determination by an *ab initio* approach and complementary solid-state ^{19}F NMR and BET studies are performed. This work and the effect of the solvent on the network topology will be discussed in a forthcoming paper.

3. Conclusion

This paper evidences the temperature effect on the network dimensionality. In the case of hybrid fluorides associating zinc cations and aminotetrazole, four new compounds with various dimensionalities are identified for a narrow domain of synthesis temperature (120–140 °C): higher the temperature, higher the network dimensionality and the aminotetrazole decomposition. $[\text{NH}_4]\cdot(\text{Zn}_4\text{F}_5(\text{amtetraz})_4)\cdot 3\text{H}_2\text{O}$ (**4**) displays an anionic 3D framework with square cavities in which ammonium cations and water

molecules are located. The loss of H_2O and NH_4F leads to a porous neutral network with an expected $\text{ZnF}(\text{amtetraz})$ formula containing unsaturated metal sites. The crystalline intermediate is currently studied in order to determine its structure and to evaluate the gas uptake capacity. Furthermore, we are currently investigating the luminescence of these new materials as it is already shown in Zn^{2+} hybrid materials [31]. Subsequent papers will focus on these issues.

4. Experimental

4.1. Synthesis

The starting reactants were ZnF_2 ($\geq 99\%$, Alfa Aesar), 4% hydrofluoric acid solution '4% HF' (2.28 mol L^{-1}) prepared from '40% HF' (HF Riedel de Haen, 22.8 mol L^{-1}), 5-aminotetrazole monohydrate '*Hamtetraz*· H_2O ' (99%, Alfa Aesar) and acetonitrile solvent 'ACN' (Sigma–Aldrich, 19.0 mol L^{-1}). All compounds were solvothermally synthesized under autogenous pressure in Teflon-lined Parr type autoclaves for 72 h. They were prepared from the same starting mixture: ZnF_2 (78 mg, 0.75 mmol), 4% HF (2.634 mL, 6 mmol), *Hamtetraz*· H_2O (78 mg, 0.75 mmol) and ACN (5 mL, 45 mmol) in molar proportions 1/8/1/60. Only the synthesis temperature was changed to obtain four new complexes from 120 °C to 140 °C. All resulting products were washed with ACN, filtered and dried at room temperature. For each preparation, X-ray diffraction was used to find the known phases (EVA software) but numerous peaks were not indexed. Then, crystals were selected to identify the new phases. The comparison of simulated and experimental diffraction patterns show that **1** and **2** are predominant at 120 °C, **3** at 130 °C and **4** at 140 °C (Fig. S1). It must be noted that in these conditions, no phase is pure: the crystalline powders are a mixture of hybrid phases, contaminated with impurities, ZnF_2 , $\text{ZnF}_2\cdot 4\text{H}_2\text{O}$ or $[\text{NH}_4]\cdot(\text{ZnF}_3)$ issued from the aminotetrazole decomposition at high temperature. In order to obtain pure phases, several experiments were carried out in a CEM microwave oven (MARS 5) and Teflon lined autoclaves at $T = 160$ °C during 1 h. Despite attempts to achieve phase purity for **1** and **2** by

modification of the nature of reactants and the synthesis temperature, only **3** and **4** were obtained pure. Pure $\text{Zn}_3\text{F}_5(\text{H}_2\text{O})_2(\text{amtetraz})$ (**3**) appeared from a mixture of 156 mg ZnF_2 (1.5 mmol), 5.27 mL HF 4% (12 mmol), 4 mL H_2O (222 mmol), 5.75 mL ACN (90 mmol), 156 mg $\text{Hamtetraz}\cdot\text{H}_2\text{O}$ (1.5 mmol) and 250 μL NH_3 (Prolabo, 16.5 molL⁻¹, 4.1 mmol). The replacement of the solvent mixture 4 mL H_2O /5.75 mL ACN by 2.5 mL H_2O /7.25 mL ACN led to pure $[\text{NH}_4]\cdot(\text{Zn}_4\text{F}_5(\text{amtetraz})_4)\cdot 3\text{H}_2\text{O}$ (**4**). The crystalline purity of **3** and **4** was confirmed by X-ray powder diffraction (Fig. S2).

4.2. Single crystal X-ray structure determination

Crystals were selected under polarizing optical microscope and mounted on MicroMount needles (MiTiGen) for single-crystal X-ray diffraction experiments. X-ray intensity data were collected on a Bruker APEX II Quazar diffractometer (4 circle Kappa goniometer, CCD detector) using 1 μs microfocus source (Mo- K_α radiation with $\lambda = 0.71073 \text{ \AA}$) at 296 K. The structure solutions were obtained by direct methods, developed by successive difference Fourier syntheses, and refined by full-matrix least-squares on all F^2 data using SHELX program suite [32] in Bruker APEX2 interface. For **4**, the twin operator (TWIN 1 0 0 0 $\bar{1}$ 0 0 0 $\bar{1}$) decreased the reliability factor from $R_1 = 0.2125$ to 0.0513. Small residual density maxima observed for the final structures of **2** and **4** were not resolved in spite of other twinning treatments.

4.3. Thermal characterization by TGA and X-ray thermodiffraction

The thermogravimetric experiments were carried out with a thermoanalyzer SETARAM TGA 92 under air flow with a heating rate of 2 °C min⁻¹ from room temperature up to 900 °C. The air atmosphere was chosen to avoid a sublimation of metal fluoride during the thermal decomposition. X ray thermodiffraction (HT-XRD) was performed under air flow in an Anton Parr XRK 900 high temperature furnace with a Panalytical X'Pert Pro diffractometer (CuK α radiation). The samples were heated from 40 °C to 600 °C at a heating rate of 10 °C min⁻¹. X-ray diffraction patterns were recorded in the 5–60° range with a scan time of 10 min at 10 °C intervals from room temperature to 400 °C and 50 °C intervals from 400 °C to 600 °C.

4.4. Infrared spectroscopy

The presence of ammonium cations in **4** and their loss as a function of the temperature was followed by IR spectroscopy. The powder was heated at a heating rate of 3 °C min⁻¹ from room temperature to $T \leq 300 \text{ °C}$ under air. IR spectra were collected (20 °C intervals) at room temperature between 40 cm⁻¹ and 4000 cm⁻¹ with a scan time of 10 min with an ALPHA FT-IR Spectrometer.

Appendix A. Supplementary data

Supplementary data associated with this article can be found, in the online version, at <http://dx.doi.org/10.1016/j.jfluchem.2016.07.003>.

References

- [1] S.-L. Li, Q. Xu, *Energy Environ. Sci.* 6 (2013) 1656–1683.
- [2] P. Horcajada, T. Chalati, C. Serre, B. Gillet, C. Sebrie, T. Baati, J.F. Eubank, D. Heurtaux, P. Clayette, C. Kreuz, J.-S. Chang, Y.K. Hwang, V. Marsaud, P.-N. Bories, L. Cynober, S. Gil, G. Férey, P. Couvreur, R. Gref, *Nat. Mater.* 9 (2010) 172–178.
- [3] J. Lee, O.K. Farha, J. Roberts, K.A. Scheidt, S.T. Nguyen, J.T. Hupp, *Chem. Soc. Rev.* 38 (2009) 1450–1459.
- [4] S. Ma, H.-C. Zhou, *Chem. Commun.* 46 (2010) 44–53.
- [5] M.P. Suh, H.J. Park, T.K. Prasad, D. Lim, *Chem. Rev.* 112 (2012) 782–835.
- [6] Y. Peng, V. Krungleviciute, I. Eryazici, J.T. Hupp, O.K. Farha, T. Yildirim, *J. Am. Chem. Soc.* 135 (2013) 11887–11894.
- [7] K. Sumida, D.L. Rogov, J.A. Mason, T.M. McDonald, E.D. Bloch, Z.R. Herm, T.-H. Bae, J.R. Long, *Chem. Rev.* 112 (2012) 724–781.
- [8] S. Qiu, M. Xue, G. Zhu, *Chem. Soc. Rev.* 43 (2014) 6116–6140.
- [9] H. Furukawa, N. Ko, Y.B. Go, N. Aratani, S.B. Choi, E. Choi, A.O. Yazaydin, R.Q. Snurr, M. O'Keeffe, J. Kim, O.M. Yaghi, *Science* 329 (2010) 424–428.
- [10] M. Dinca, J.R. Long, *Angew. Chem. Int. Ed.* 47 (2008) 6766–6779.
- [11] S. Kitagawa, R. Kitaura, S. Noro, *Angew. Chem. Int. Ed.* 43 (2004) 2334–2375.
- [12] D. Zhao, Daren J. Timmons, D. Yuan, H.-C. Zhou, *Acc. Chem. Res.* 44 (2011) 123–133.
- [13] F. Millange, C. Serre, G. Férey, *Chem. Commun.* (2002) 822–823.
- [14] H. Li, M. Eddaoudi, M. O'Keeffe, O.M. Yaghi, *Nature* 402 (1999) 276–279.
- [15] W. Ouellette, B.S. Hudson, J. Zubietta, *Inorg. Chem.* 46 (2007) 4887–4904.
- [16] M.P. Suh, Y.E. Cheon, E.Y. Lee, *Chem. Eur. J.* 13 (2007) 4208–4215.
- [17] V. Pimenta, J. Lhoste, A. Hémon-Ribaud, M. Leblanc, J.-M. Grenèche, L. Jouffret, A. Martel, G. Dujardin, V. Maisonnette, *Cryst. Growth Des.* 15 (2015) 4248–4255.
- [18] C. Su, A.M. Goforth, M.D. Smith, P.J. Pellechia, H.C. Zur Loye, S. Carolina, *J. Am. Chem. Soc.* (2004) 3576–3586.
- [19] A.M. Goforth, C.Y. Su, R. Hipp, R.B. MacQuart, M.D. Smith, H.C. Zur Loye, *J. Solid State Chem.* 178 (2005) 2511–2518.
- [20] A.X. Zhu, J. Bin Lin, J.P. Zhang, X.M. Chen, *Inorg. Chem.* 48 (2009) 3882–3889.
- [21] A. Cadiau, C. Martineau, F. Taulelle, K. Adil, *J. Fluorine Chem.* 150 (2013) 104–108.
- [22] V. Pimenta, Q.H.H. Le, L. Clark, J. Lhoste, A. Hémon-Ribaud, M. Leblanc, J.-M. Grenèche, G. Dujardin, P. Lightfoot, V. Maisonnette, *Dalton Trans.* 44 (2015) 7951–7959.
- [23] M. Smida, J. Lhoste, V. Pimenta, A. Hémon-Ribaud, L. Jouffret, M. Leblanc, M. Dammak, J.-M. Grenèche, V. Maisonnette, *Dalton Trans.* 42 (2013) 15748–15755.
- [24] S. Aguado, C. Aquino, C. Martineau, Y.V. Ryabchikov, V. Lysenko, E.A. Quadrelli, J. Canivet, D. Farrusseng, *CrystEngComm* 15 (2013) 9336–9339.
- [25] A. Cadiau, C. Martineau, M. Leblanc, V. Maisonnette, A. Hémon-Ribaud, F. Taulelle, K. Adil, *J. Mater. Chem.* 21 (2011) 3949–3951.
- [26] S. Bauer, C. Serre, T. Devic, P. Horcajada, J. Marrot, G. Férey, N. Stock, *Inorg. Chem.* 47 (2008) 7568–7576.
- [27] P.M. Forster, A.R. Burbank, C. Livage, G. Férey, A.K. Cheetham, *Chem. Commun.* (2004) 368–369.
- [28] A.A. Paletsky, N.V. Budachev, O. Korobeinichev, *Kinet. Catal.* 50 (2009) 627–635.
- [29] N. Piekielek, M.R. Zachariah, *J. Phys. Chem. A* 116 (2012) 1519–1526.
- [30] N.M. Laptash, *J. Fluorine Chem.* 105 (2000) 59–64.
- [31] E.-C. Yang, H.-K. Zhao, B. Ding, X.-G. Wang, X.-J. Zhao, *Cryst. Growth Des.* 7 (2007) 2009–2015.
- [32] G.M. Sheldrick, SHELXL-2014, Program for Crystal Structure Determination, Göttingen University, Germany, 2014.